Biophysical Journal Volume 107 September 2014 1146–1155

Article

# Carbohydrate Conformation and Lipid Condensation in Monolayers Containing Glycosphingolipid Gb3: Influence of Acyl Chain Structure

Erik B. Watkins,[1,*] Haifei Gao,[2,3,4] Andrew J. C. Dennison,[1,5] Nathalie Chopin,[2,3,4] Bernd Struth,[6] Thomas Arnold,[7] Jean-Claude Florent,[2,3,4] and Ludger Johannes[2,3,4]

[1]Institut Laue-Langevin, 38042 Grenoble Cedex 9, France; [2]Institut Curie, Centre de Recherche, 75248 Paris Cedex 5, France; [3]CNRS UMR3666, 75005 Paris, France; [4]INSERM U1143, 75005 Paris, France; [5]Department of Physics and Astronomy, Box 516. SE-751 20, Uppsala University, Uppsala, Sweden; [6]HASYLAB at DESY, Notkestrasse 85 D-22603, Hamburg, Germany; and [7]Diamond Light Source, Harwell Science and Innovation Campus, Chilton, United Kingdom

ABSTRACT Globotriaosylceramide (Gb3), a glycosphingolipid found in the plasma membrane of animal cells, is the endocytic receptor of the bacterial Shiga toxin. Using x-ray reflectivity (XR) and grazing incidence x-ray diffraction (GIXD), lipid monolayers containing Gb3 were investigated at the air-water interface. XR probed Gb3 carbohydrate conformation normal to the interface, whereas GIXD precisely characterized Gb3's influence on acyl chain in-plane packing and area per molecule (APM). Two phospholipids, 1,2-distearoyl-*sn*-glycero-3-phosphocholine (DSPC) and 1,2-dipalmitoyl-*sn*-glycero-3-phosphoethanolamine (DPPE), were used to study Gb3 packing in different lipid environments. Furthermore, the impact on monolayer structure of a naturally extracted Gb3 mixture was compared to synthetic Gb3 species with uniquely defined acyl chain structures. XR results showed that lipid environment and Gb3 acyl chain structure impact carbohydrate conformation with greater solvent accessibility observed for smaller phospholipid headgroups and long Gb3 acyl chains. In general, GIXD showed that Gb3 condensed phospholipid packing resulting in smaller APM than predicted by ideal mixing. Gb3's capacity to condense APM was larger for DSPC monolayers and exhibited different dependencies on acyl chain structure depending on the lipid environment. The interplay between Gb3-induced changes in lipid packing and the lipid environment's impact on carbohydrate conformation has broad implications for glycosphingolipid macromolecule recognition and ligand binding.

## INTRODUCTION

Glycosphingolipids (GSLs), a class of lipid consisting of a ceramide linked to a carbohydrate moiety, are cell surface receptor molecules that play a role in diverse biological processes including specific recognition of macromolecules, intercellular trafficking, cell adhesion, and signal transduction (1). Primarily located within the outer leaflet of animal cell membranes, a broad species and concentration distribution exists across differing cell types. Naturally occurring species exhibit varied carbohydrate and hydrocarbon motifs providing a range of different biofunctionality. Specific recognition of the heterogeneous carbohydrate motif, which extends perpendicular to the membrane into the extracellular space, provides variable ligand binding affinities and cellular signaling functions (2). GSLs also exhibit heterogeneous fatty acid content resulting in variable self-aggregation and packing properties for different species in the membrane (3). Although the majority of phospholipid species have 16 or 18 carbon chains, typical GSL tails have significantly longer acyl chains. The longer chain length may serve to promote extension of the carbohydrate into the extracellular space and to enhance ligand binding (4). Alternatively, longer acyl chains can interdigitate into the opposing leaflet providing a potential signal transduction mechanism (5). In fact, evidence for both conformations depending on either the acyl chain structure or the properties of the local membrane environment suggests that both biological functions may be relevant (6). Variable acyl chain structure also provides the capability for lateral segregation and partitioning within membrane microdomains. In general, GSLs and phospholipids do not phase separate but self-organize to form a mixture with GSL-enriched clusters (1). In a cellular context, GSLs are enriched in compositionally distinct microdomains known as lipid rafts, which exhibit tighter molecular packing and serve as platforms for specific biological function (7,8). Recent work suggest GSL interactions stabilize raft platforms and impact biological function in terms of intracellular trafficking and cytotoxicity following bacterial toxin binding (9,10). This indicates that the construction of raft environments with defined changes in the local lipid composition may regulate GSL carbohydrate conformation and function. Globotriaosylceramide (Gb3) is a GSL with a carbohydrate structure consisting of two galactose and one glucose residue and

*Submitted April 15, 2014, and accepted for publication July 1, 2014.*

*Correspondence: erik.b.watkins@gmail.com

Nathalie Chopin's present address is Laboratoire Biotechnologies et Molécules Marines, Ifremer, France.

Erik Watkins' present address is Lujan Neutron Scattering Center, Los Alamos National Laboratory, Los Alamos, New Mexico 87545, USA. Email: ebw@lanl.gov.

Editor: Ka Yee Lee.



0006-3495/14/09/1146/10 $2.00

http://dx.doi.org/10.1016/j.bpj.2014.07.023

specific binding affinity for Shiga toxin. Like all GSLs, Gb3 exhibits acyl chain heterogeneity with a predominance of long chain species and the different structures impact ligand binding affinity. For example, Gb3 possessing long unsaturated acyl chains were found to preferentially bind Shiga toxin (11). Gb3's hydrocarbon structure was also found to influence the formation of tubular invaginations and the initiation of receptor-mediated endocytosis with long unsaturated acyl chain preferentially forming tubular invaginations (12). Furthermore, for related toxin-GSL interactions between cholera and GM1, cell intoxication was favored for GSLs with long unsaturated acyl chain structures (13).

In this work, x-ray reflectivity (XR) and grazing incidence x-ray diffraction (GIXD) were used to investigate mixed monolayers composed of phospholipids and Gb3 at the air-water interface. Lipid monolayers provide a versatile membrane model permitting the application of surface-sensitive scattering techniques as well as external control of surface pressure ($\pi$). Exploiting these advantages, monolayers composed of 4:1 mixtures of phospholipid and Gb3 were studied over a range of biologically relevant surface pressures, $20 < \pi < 40$ mN/m. The 4:1 molar ratio ensured that, on average, each Gb3 was surrounded by phospholipid neighbors and was used to model the enhanced GSL concentration within lipid rafts. Phospholipids with saturated hydrocarbon chains were selected to mimic the tighter packing characteristic of rafts and to enable GIXD measurements. Two structurally distinct phospholipids, 1,2-distearoyl-*sn*-glycero-3-phosphocholine (DSPC) and 1,2-dipalmitoyl-*sn*-glycero-3-phosphoethanolamine (DPPE), were used to study Gb3 packing in different lipid environments. These lipids exhibit chemical differences in both their hydrocarbon and hydrophilic headgroups allowing multiple contributions to Gb3 packing in mixed monolayers to be investigated. Specifically, the role of the phospholipid hydrocarbon chain length was investigated by comparing Gb3 packing with longer chain DSPC lipids (18:0) to shorter chain DPPE lipids (16:0). Additionally, the impact on Gb3 conformation due to steric interactions between the carbohydrate and either the phosphoethanolamine (PE) or the larger phosphocholine (PC) headgroups was compared. Although this lipid choice facilitated the investigation of varied membrane environments, the specific impact of each contribution to monolayer order could not always be unambiguously identified. Finally, the role of Gb3's structure was investigated by comparing mixtures containing Gb3 extracted from porcine red blood cells (pRBC) to synthetic Gb3 analogs with uniquely defined acyl chain structures: 22:0, 22:1, 14:0, and lyso Gb3 (see Fig. 1 *B*). XR was used to measure the out-of-plane structure of the monolayers and characterize the extension and conformation of Gb3's carbohydrate moiety. Using GIXD, the in-plane packing of the acyl chains and average area per molecule (APM) of the monolayers were characterized. Observation of a Gb3-induced APM condensation may shed light on a mechanism for Gb3 partitioning in membrane microdomains and a tendency to induce raft formation. Additionally, perturbations to the lateral ordering may represent the onset of a tilt textured lipid phase with implications for the induction receptor-mediated endocytosis.

## MATERIALS AND METHODS

### Lipid monolayer preparation

DSPC and DPPE were obtained from Avanti Polar Lipids (Alabaster, AL). Gb3 extracted from pRBC was obtained from Matreya LLC (Pleasant Gap, PA). Lipids from these sources were used without further purification. Gb3 analogs with variable acyl chain moieties (22:0, 22:1, 14:0, and lyso) were synthesized from the glycosyl conjugation of peracetylated globotriosyl trichloroacetimidate and 3-Obenzoyloxyazidosphingosine. Detailed description of the synthesis can be found in the Supporting Material. All synthesized analogs were purified by chromatography before use.

Lipids were dissolved in HPLC grade chloroform or 9:1 chloroform/methanol and mixed to yield 1 mg/ml monolayer spreading solutions. The solutions used were pure components or 4:1 mole ratio mixtures of phospholipid/Gb3. Monolayers were prepared by spreading from solution onto pH 7.4 buffered water in a Langmuir trough held at 20°C. Buffers were made from ultrapure water (resistivity $\geq$18 MΩcm) and PBS Dulbecco without $Ca^{2+}$ or $Mg^{2+}$ (Sigma Aldrich, St. Louis, MO). After solvent evaporation, monolayers were compressed at a rate of 10–15 $cm^2$/min to obtain $\pi$-area isotherms or to maintain a desired $\pi$ for Brewster angle microscopy (Nanofilm EP3) or x-ray scattering measurements.

### X-ray scattering measurements

Synchrotron XR and GIXD measurements were performed at the BW1 beamline at HASYLAB (Hamburg, Germany) and at the I-07 beamline at Diamond Light Source. (Didcot, United Kingdom). For BW1 experiments, a beryllium monochromater yielded $\lambda = 1.30$Å x-rays. By tilting the monochromater crystal, the beam was deflected to change the angle of incidence. In XR experiments, a NaI scintillation point detector was used. In GIXD experiments, an evanescent wave was generated by an incident beam striking the water surface at an angle corresponding to $q_z = 0.85\ q_c$ where $q_c = 0.0219$ Å$^{-1}$. Diffracted intensities for GIXD experiments were measured using a vertically oriented one-dimensional position sensitive detector (PSD) with an acceptance of $0 < q_z < 0.9$ Å$^{-1}$. Soller collimation mounted in front of the PSD provided a horizontal resolution of $\Delta q_{xy} = 0.0084$ Å$^{-1}$ and the detector was scanned over $2\theta_{xy}$, the angle between the incident and diffracted beam projected onto the horizontal plane, to yield a $q_z$ vs. $q_{xy}$ intensity distribution. For the I-07 experiments, the energy was set to 12.5 keV yielding a x-ray beam with wavelength $\lambda = 0.992$ Å. The incident angle of the x-rays on the water surface was adjusted using a double-crystal deflection scheme (14). XR measurements were performed using a two-dimensional (2D) Pilatus 100 K PSD with regions of interest defined such that reflected and background intensities were collected simultaneously. GIXD measurements were performed at an incident angle corresponding to $q_z = 0.85\ q_c$ and $q_z$ vs. $q_{xy}$ intensity distributions were measured with the 2D PSD and slits to define a pinhole focusing geometry. A temperature-controlled Langmuir trough was mounted on each instrument and used to control $\pi$ throughout the experiments. The troughs were contained within helium gas purged enclosures and translated to minimize beam damage. Overall, XR and GIXD data obtained on each instrument were of comparable quality and statistics.

### XR

XR measures the ratio of reflected to incident intensity as a function of the vertical momentum transfer vector $q_z = 4\pi \sin\theta/\lambda$ where $\theta$ is the incident

angle of the x-rays on the surface and $\lambda$ is the x-ray wavelength (Fig. 1 *A*, *inset*). Intensities were collected over the range $0.01 < q_z < 0.7$ Å$^{-1}$, background subtracted, and normalized to unity. Data have been presented multiplied by $q_z^4$ with error bars representing statistical errors. The reflectivity curve can be analyzed to obtain the in-plane averaged electron density distribution normal to the interface. To accomplish this, the monolayer was described as a series of boxes parameterized by their thickness, electron density, and interfacial roughness, and the Parratt formalism was employed to calculate the reflected intensity from the model (15). In general, our approach used the simplest possible model to describe the data. For pure lipid monolayers, the data were modeled using a box representing hydrocarbon tails and a second box representing hydrophilic headgroups. For Gb3 monolayers three boxes were used with two boxes representing the hydrocarbon tails and a third box representing the polar moieties and carbohydrate groups. Three boxes were also used to model mixed monolayers with one box representing the tails, one for the polar headgroups, and a third for the carbohydrates. A Levenburg-Marquardt minimization algorithm was used to vary the box model parameters to obtain the solution corresponding to the lowest $\chi^2$ value. Typical reduced $\chi^2$ values for the fits presented were <10.

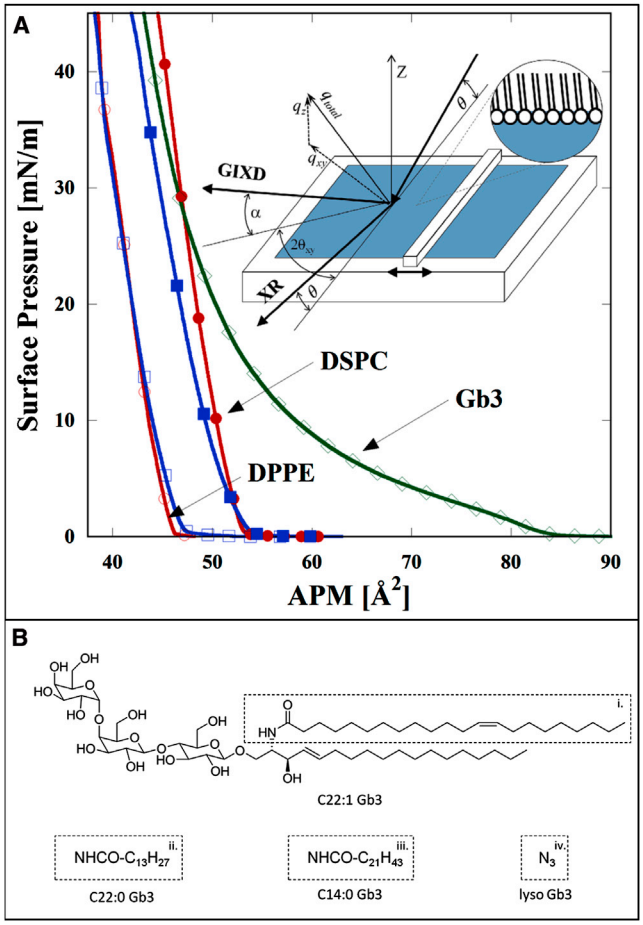


FIGURE 1 (*A*) $\pi$-a isotherms of 4:1 mixed monolayers compared to the structure of single-component monolayers of DSPC (*red solid circles*), DPPE (*red open circles*), and pRBC Gb3 (*green diamonds*). The 4:1 DSPC/Gb3 mixture (*blue solid squares*) shows smaller APM than the single-component monolayers. The 4:1 DPPE/Gb3 mixture (*blue open squares*) approximately matches the DPPE isotherm. Inset shows lipid monolayers at the air-water interface and the scattering geometry used for XR and GIXD measurements. (*B*) Structure of the synthetic Gb3 analogous used in this study. To see this figure in color, go online.

## GIXD

GIXD probes the lateral ordering and in-plane packing of lipid tails in the monolayer using an evanescent wave to amplify surface sensitivity (Fig. 1 *A*, *inset*). Diffraction results when the 2D ordering within the film satisfies the Bragg condition $n\lambda = 2d\sin\theta$. Diffracted intensities were recorded as a function of both $q_z = 2\pi \sin\alpha_f/\lambda$ where $\alpha_f$ is the out-of-plane angle of the diffracted beam and $q_{xy} \approx 4\pi \sin(2\theta_{xy}/2)\lambda$ where $2\theta_{xy}$ is the angle between the incident and diffracted beam projected onto the horizontal plane (16). Following background subtraction, the data were integrated over $q_z$ to yield intensity Bragg peak profiles. Pseudo-Voight functions were used to fit the Bragg peaks. Peak positions correspond to the *d*-spacings in the 2D lattice and were used to obtain the unit cell packing parameters associated with the lipid chains (17).

# RESULTS

## Pressure-area isotherms

Surface pressure versus molecular area ($\pi$-a) isotherms provide information about lipid phase behavior and average APM of monolayers at the air-water interface. Isotherms were measured for DSPC, DPPE, and Gb3 monolayers as well as for 4:1 phospholipid/Gb3 mixtures (Fig. 1 *A*). Three repeat measurements were performed and variation in the APM was in the range of 5–10%. Consistent with isotherms of other GSL monolayers, the Gb3 isotherm showed changes to $\pi$ at APM >80 Å$^2$ (18–20). The long-range interactions can be attributed to the carbohydrate hydration shell and following compression the APM converged to 40–50 Å$^2$ consistent with PC lipids (21,22). In contrast, isotherms of DPPE or DSPC monolayers exhibited a much steeper increase in $\pi$ resulting in ~8 Å$^2$ larger APM for DSPC due to molecular tilt arising from the size mismatch between PC and the acyl chain cross sections (23). Substantial differences were observed between DSPC and the DSPC/Gb3 isotherms with the mixture exhibiting a smaller APM. On the other hand, the $\pi$-a isotherm of the DPPE/Gb3 mixture can, for the most part, be superimposed onto the isotherm of a single-component DPPE monolayer. $\pi$-a isotherms of the mixtures were not a linear combination of the isotherms of the components indicating miscibility (24). In both cases, the isotherms indicated that a gas-condensed phase transition occurred immediately after liftoff. Furthermore, no lateral domain formation was observed within the mixtures using Brewster angle microscopy. Isotherms and Brewster angle microscopy measurements performed on monolayers containing the Gb3 analogs yielded qualitatively similar results.

## XR: Gb3 extracted from porcine RBC

The out-of-plane structure of phospholipid, pRBC Gb3, and 4:1 phospholipid/Gb3 monolayers were characterized at 30 mN/m using XR (Fig. 2). The in-plane averaged electron density distribution, $\rho_{e^-}$, clearly distinguished the hydrocarbon tails, the relatively electron-rich polar headgroups of the phospholipids, and the Gb3 carbohydrate moieties. From these $\rho_{e^-}$ distributions, the average lipid APM, changes in

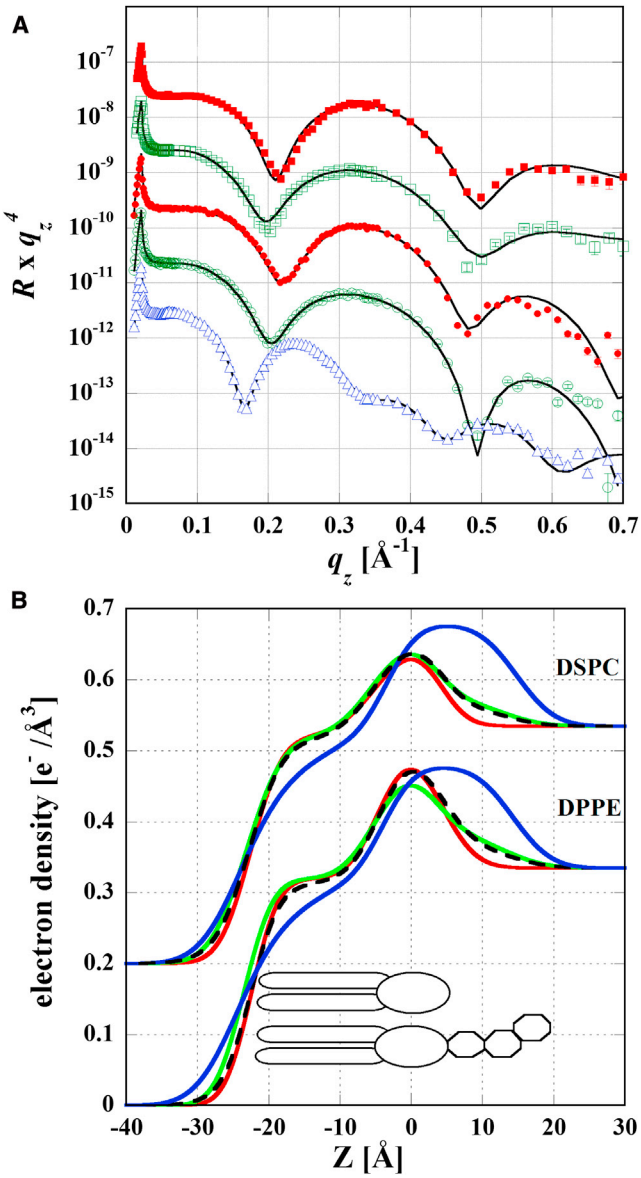


FIGURE 2 Out-of-plane structures of 4:1 mixtures compared to single-component monolayers. (*A*) XR data and fits multiplied by $q_z^4$ and offset vertically for clarity. From top to bottom, curves correspond to 30 mN/m monolayers of DSPC, 4:1 DSPC/Gb3, DPPE, 4:1 DPPE/Gb3, and pRBC Gb3. (*B*) Electron density profiles matching the fits in (*A*) with headgroups centered at $z = 0$. The inset depicts the location of lipid tails, headgroups, and Gb3 carbohydrates. Red lines correspond to $\rho_{e^-}$ of the pure lipids, blue lines to the Gb3 monolayer, and green lines to the mixtures. Profiles for DSPC are offset vertically by $0.2e^-/\text{Å}^3$ for clarity. 4:1 linear combinations of the pure lipid and pure Gb3 profiles (*dashed lines*) reproduce the electron density distribution of the DSPC/Gb3 mixture but not the DPPE/Gb3 mixture. To see this figure in color, go online.

molecular tilt, and Gb3 carbohydrate conformation can be estimated. XR measurements at 20 mN/m and 40 mN/m showed small changes consistent with a decrease in out-of-plane tilt as $\pi$ increased (see the Supporting Material). Complementary in-plane structure on these systems will be presented in the section on GIXD.

For the DSPC monolayer, the center of the PC headgroups corresponds to a $\rho_{e^-}$ maximum at $z = 0$. The $\rho_{e^-}$ shoulder to the left of this maximum corresponds to the hydrocarbon tails and the distribution plateaus to the right at the $\rho_{e^-}$ of water. The DPPE monolayer exhibited qualitatively similar features with a higher headgroup $\rho_{e^-}$ indicative of tighter packing. A quantitative estimate of the APM can be obtained from the thickness and $\rho_{e^-}$ of the lipid tail parameters using the equation $\text{APM} = n_{e^-}/T_{HG}\rho_{e^-}$ where $T_{HG}$ is the thickness of the box representing the tails, and $n_{e^-}$ is the number of lipid tail electrons. Here, we define all atoms up to and including the carbonyls as the headgroup and the remaining hydrocarbons as the lipid tails. Using this approach, the average APM was calculated to be 49Å$^2$ for the DSPC bilayer and 42Å$^2$ for the DPPE bilayer in good agreement with the literature and GIXD results reported in this work (25,26). Compared to DPPE and DSPC, the $\rho_{e^-}$ distribution of a pRBC Gb3 monolayer has a broader high $\rho_{e^-}$ region corresponding to both the polar headgroup and the carbohydrate. The lower density tail region indicates more disordered packing of the lipid chains. Two boxes were used to model the Gb3 tails: a higher density region adjacent to the headgroup composed of both ceramide and acyl chains and a lower density region representing the portion of the longer acyl chains extending above the ceramide. Using the same approach as above, an APM of 49 Å$^2$ was obtained that is consistent with the isotherm. For the DSPC/Gb3 mixture, the carbohydrate $\rho_{e^-}$ is clearly seen extending ~10 Å into the water. Additionally, the lipid tail region is thicker than the DSPC monolayer suggesting a decreased out-of-plane tilt. A linear combination of the pure component electron density profiles closely reproduced the modeled $\rho_{e^-}$ of the mixture. This indicates no dramatic rearrangement of the out-of-plane DSPC structure upon incorporation of Gb3 and that the carbohydrate conformation in the mixture resembles that of the pure Gb3 monolayer. However, these measurements are not sensitive to more subtle changes in the out-of-plane structure that may be associated with modest APM condensation. In the case of the DPPE/Gb3 mixture, the carbohydrate $\rho_{e^-}$ is also clearly seen extending into the water and the lipid tail region is thicker. Additionally, the PE headgroup $\rho_{e^-}$ is diminished due to either substitution of PE with the less electron-rich polar region of Gb3 or disordering of the headgroups. The 43 Å$^2$ APM estimated from the XR box model is consistent with a linear combination of the pure component APM obtained via the same method. However, a linear combination of the $\rho_{e^-}$ does not reproduce the measured distribution of the DPPE/Gb3 mixture. Although the carbohydrate $\rho_{e^-}$ can be approximated by the linear combination, there are significant differences in the lipid tail and headgroup regions. This suggests that incorporation of Gb3 into a DPPE monolayer results in significant perturbations to its out-of-plane structure and that the carbohydrate conformation may not be maintained relative to the pure Gb3 monolayer.

## XR: influence of Gb3 tail structure

Fig. 3 *A* compares the out-of-plane electron density distribution of 30 mN/m monolayers composed of each of the Gb3 analogs (22:0, 22:1, 14:0, and lyso) to the pRBC Gb3 mixture. Corresponding XR data and fits can be found in the Supporting Material. Structural differences can be discerned both in the tail and carbohydrate regions. Centered at $z = 0$, the $\rho_{e^-}$ maximum corresponds to both the polar headgroup and carbohydrates of Gb3. This region is significantly broader (17 Å) for the pRBC Gb3 mixture than for any of the single-component Gb3 species (11–14 Å) and may reflect different out-of-plane packing geometries for the various tail moieties within the mixture. With the exception of the 22:1 Gb3 monolayer, the maxima have approximately equal $\rho_{e^-}$ suggesting similar average APM. The reduced 22:1 Gb3 maximum may signify more disordered packing of the unsaturated chains and a larger average APM. In general, differences in the thickness of the hydrocarbon tails correlated to the length of the Gb3 acyl chains. The unsaturated Gb3 species, with a tail thickness equal to 14:0 Gb3, did not follow this trend also suggesting an increased APM. Additionally, pRBC and the 22:0 Gb3 had comparable tail thicknesses but difference in the $\rho_{e^-}$ distribution indicated the various tail moieties within the mixture altered the out-of-plane packing. APM calculations based on the tail region $\rho_{e^-}$ yielded values of 49 Å$^2$, 45 Å$^2$, 51 Å$^2$, 40 Å$^2$, 35 Å$^2$ for the pRBC Gb3, 22:0 Gb3, 22:1 Gb3, 14:0 Gb3, and lyso Gb3, respectively. Measurements of the Gb3 mixture at 20 and 40 mN/m exhibited small changes consistent with decreased lipid tilt at higher $\pi$.

Structures obtained from 4:1 mixtures of DSPC and the different Gb3 analogs are shown in Fig. 3 *B*. The profiles correspond to monolayers at 30 mN/m with the exception of 22:1 Gb3 which was measured at 40 mN/m. In all cases, the carbohydrate region extended 10–15 Å from the center of the headgroups, whereas the integrated carbohydrate $\rho_{e^-}$ varied depending on Gb3 acyl chain structure. Adjusted for small changes in APM, the integrated $\rho_{e^-}$ correlates to the carbohydrate volume penetrating into the water. Relative to the DSPC monolayer, the lipid tail region thickness increased for all mixtures with the exception of lyso Gb3. Contributions to this increased thickness can be attributed to either the longer Gb3 acyl chain length or a decrease in lipid tilt.

Fig. 3 *C* compares the out-of-plane structure of 4:1 DPPE/Gb3 monolayers at 20 mN/m with variable Gb3 acyl chain structures. As in the case of the DSPC/Gb3 mixtures, the $\rho_{e^-}$ associated with the carbohydrates extended 10–15 Å into the water. Furthermore, the peak in the $\rho_{e^-}$ profile representing the PE headgroups is significantly reduced in the mixtures compared to the DPPE monolayer. The decrease, which was less pronounced for the pRBC Gb3, can be attributed to either reduced $\rho_{e^-}$ of the Gb3 headgroup relative to PE or a decreased average APM of the mixture. Variations due to the Gb3 acyl chain structure were observed in the carbohydrate region of the monolayer. The $\rho_{e^-}$ associated with carbohydrates was greater for pRBC Gb3, intermediate for 22:0 Gb3, and significantly less for the other three species. As mentioned for the case of DSPC, the variability of the carbohydrate $\rho_{e^-}$ results from different solvent accessible carbohydrate volumes. Small differences in the thickness of the hydrocarbon region were also observed.

## GIXD: Gb3 extracted from porcine RBC

In-plane packing of lipid hydrocarbon chains within phospholipid, pRBC Gb3, and phospholipid/Gb3 monolayers was investigated using GIXD (Fig. 4). The diffraction from lipid chains in DSPC monolayers was compared to diffraction from 4:1 DSPC/Gb3 mixtures as a function

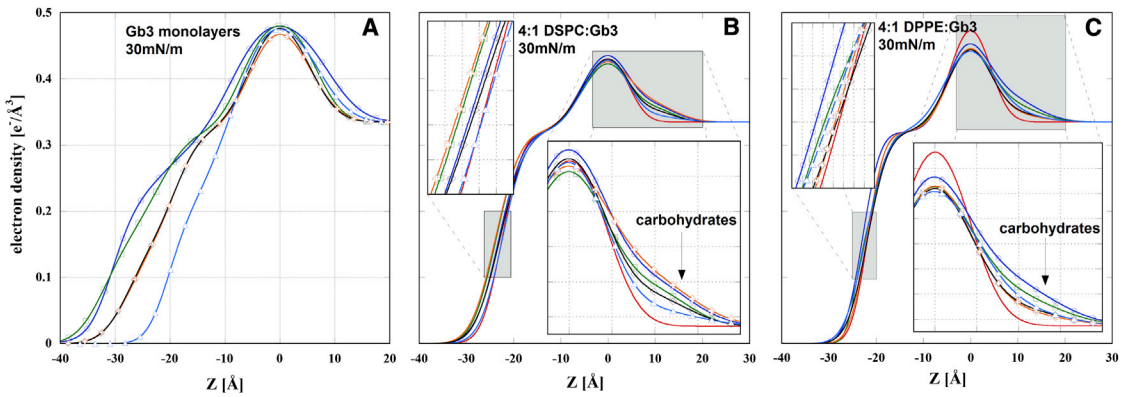


FIGURE 3 Influence of Gb3 hydrocarbon moieties on the out-of-plane monolayer structure. (*A*) Electron density profiles obtained from fitting XR data of single-component Gb3 monolayers at 30 mN/m: pRBC Gb3 mixture (*blue circles*), 22:0 Gb3 (*green squares*), 22:1 Gb3 (*orange crosses*), 14:0 Gb3 (*black diamonds*), and lyso Gb3 (*light blue triangles*). (*B*) Electron density profiles of 4:1 DSPC/Gb3 monolayers at 30 mN/m. Magnifications of the carbohydrate region and a section of the lipid tail region are shown to emphasize the influence of the different Gb3 species on monolayer structure. Electron density of a 30 mN/m DSPC bilayer (*red line*) is shown for comparison. (*C*) Electron density profiles of 4:1 DPPE/Gb3 monolayers at 20 mN/m with magnifications of the carbohydrate and tail regions. Electron density of a 20 mN/m DPPE bilayer (*red line*) is shown for comparison. To see this figure in color, go online.

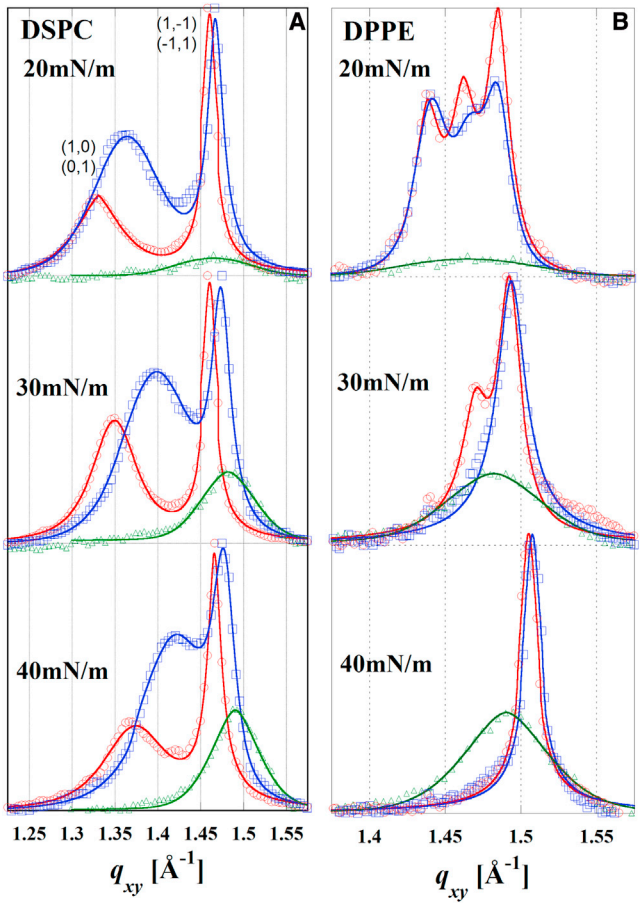


FIGURE 4 GIXD from 4:1 mixed monolayers compared to single-component monolayers. Data are presented on an arbitrary intensity scale and shifted vertically for clarity. Errors are approximated by the size of the data points and lines are fits to the data using pseudo-Voight functions. (*A*) Bragg peak profiles of DSPC monolayers (*red circles*), 4:1 DSPC/Gb3 monolayers (*blue squares*), and pRBC Gb3 monolayers (*green triangles*) at 20, 30, and 40 mN/m. DSPC and DSPC/Gb3 Bragg peaks are normalized to the high $q_{xy}$ peak intensity and the relative intensity of the Gb3 Bragg peaks is approximated. The higher $q_{xy}$ positions of DSPC/Gb3 peaks indicate a smaller APM than in single-component DSPC monolayers. (*B*) Bragg peak profiles of DPPE monolayers (*red circles*), 4:1 DPPE/Gb3 monolayers (*blue squares*), and pRBC Gb3 monolayers (*green triangles*) at 20, 30, and 40 mN/m. At 30 and 40 mN/m, the mixed monolayer Bragg peak shifts indicate smaller APM. At 20 mN/m, the relative intensity of the three mixed monolayer peaks is perturbed consistent with the emergence of lipid tilt texture. To see this figure in color, go online.

of $\pi$. A single Bragg peak was observed for Gb3 monolayers suggesting hexagonal symmetry and untilted hydrocarbon chains. The Bragg peak position shifted proportionally to $\pi$ consistent with an approximately linear decrease in APM and tighter lipid packing with increasing $\pi$. For the DSPC and DSPC/Gb3 monolayers, two Bragg peaks are clearly distinguished indicative of a distorted hexagonal lattice with lipid chains tilted toward their nearest neighbor. Again, the Bragg peak positions shift to higher $q_{xy}$ indicating smaller APM at higher $\pi$. The 4:1 DSPC/Gb3 mixture Bragg peak positions are also consistently shifted to higher $q_{xy}$ compared to the equivalent $\pi$ DSPC peaks demonstrating that incorporation of Gb3 decreased the average APM.

To obtain unit cell parameters, the Bragg peak position of Gb3 monolayer diffraction was indexed using a hexagonal unit and the resulting APM are reported in Table 1. It should be noted that the value obtained at 30 mN/m from GIXD is significantly smaller than the 49 Å$^2$ estimated using XR. Although XR averages the entire monolayer APM, GIXD only measures the APM from ordered regions. This suggests that the discrepancy in measured APM originates from the presence of nanoscale Gb3 clusters in the monolayer. For DSPC and DSPC/Gb3 monolayers the diffraction was indexed using a distorted hexagonal unit cell with nearest neighbor tilt to obtain APM (Table 1). The measured APM of the DSPC/Gb3 mixtures were consistently smaller than the values predicted by ideal mixing of the pure components.

Fig. 4 *B* shows Bragg peaks corresponding to DPPE, pRBC Gb3, and 4:1 DPPE/Gb3 monolayers at 20, 30, and 40 mN/m. At low $\pi$, three DPPE diffraction peaks were observed indicative of an oblique unit cell with tilted hydrocarbon chains. As the monolayer $\pi$ increased, the number of peaks dropped to two at 30 mN/m and to a single degenerate peak at 40 mN/m. This indicates a structural transition from tilted molecules arranged in an oblique unit cell to untilted molecules in a hexagonal unit cell. The diffraction from DPPE/Gb3 monolayers exhibited a similar transition with the untilted hexagonal phase emerging at 30 mN/m as opposed to 40 mN/m. Compared to the peak positions from DPPE diffraction, a small shift to higher $q_{xy}$ is observed for the DPPE/Gb3 mixtures suggesting smaller APM. Furthermore, at 20 mN/m a perturbation to the relative intensities of the three DPPE/Gb3 diffraction peaks in violation of the multiplicity rule is observed. Previously, similar changes in relative GIXD peak intensities have been associated with in-plane texture of lipid tilt orientations (27,28).

**TABLE 1 Influence of surface pressure ($\pi$) on lipid APM[a]**

| | $\pi$ | | |
|---|---|---|---|
| | 20 mN/m | 30 mN/m | 40 mN/m |
| Porcine Gb3 | 42.5 Å$^2$ | 41.5 Å$^2$ | 41.0 Å$^2$ |
| DSPC | 48.6 Å$^2$ | 47.6 Å$^2$ | 46.4 Å$^2$ |
| Ideal mixing[b] | 47.4 Å$^2$ | 46.4 Å$^2$ | 45.3 Å$^2$ |
| 4:1 DSPC/Gb3 | 46.8 Å$^2$ | 45.1 Å$^2$ | 44.0 Å$^2$ |
| Deviation[c] | −1.3% | −2.8% | −2.9% |
| Porcine Gb3 | 42.5 Å$^2$ | 41.5 Å$^2$ | 41.0 Å$^2$ |
| DPPE | 42.7 Å$^2$ | 41.8 Å$^2$ | 40.2 Å$^2$ |
| Ideal mixing[b] | 42.6 Å$^2$ | 41.7 Å$^2$ | 40.4 Å$^2$ |
| 4:1 DPPE/Gb3 | 42.6 Å$^2$ | 41.5 Å$^2$ | 40.1 Å$^2$ |
| Deviation[c] | 0.0% | −0.5% | −0.7% |

[a]Uncertainty in APM values is ±0.1 Å$^2$.
[b]APM for ideal mixing was calculated as a 4:1 linear combination of the single-component APM.
[c]Deviation is the percent difference between the mixed monolayer APM and the ideal mixing APM.

To obtain unit cell parameters and APM, the Bragg peak profiles were fit and indexed to the relevant unit cell based on the number of observed peaks: hexagonal (1 peak), distorted hexagonal (2 peaks), and oblique (3 peaks). The APM obtained and predictions based on ideal mixing are shown in Table 1. At 20 mN/m, no condensing effect was observed and the measured APM of the DPPE/Gb3 mixture matched the calculation based on ideal mixing. At higher pressures, the APM of the mixed monolayer indicated a condensed monolayer structure.

### GIXD: influence of Gb3 tail structure

GIXD was also used to investigate the impact of Gb3 acyl chain structure on the in-plane packing in mixed monolayers. The measured APM for each monolayer composition and the deviation of the mixed monolayer APM from an ideal mixing prediction is reported in Table 2. Diffraction was not obtained from monolayers composed of DSPC and 22:1 Gb3 due to more disordered packing of the lipid tails. In the case of DSPC mixtures containing either pRBC Gb3 or 22:0 Gb3, the lipid APM were smaller than predicted for ideal mixing. At $\pi = 20$ mN/m and $\pi = 40$ mN/m, APM condensation was also observed for DPPE mixtures containing both saturated Gb3 species with 14:0 Gb3 exhibiting greater deviation from ideal mixing. For DPPE mixtures containing 22:1 Gb3, no significant condensation of APM was observed. However, similar to the pRBC Gb3 case discussed earlier, change in the relative intensities of the peaks at 20 mN/m, in violation of the multiplicity rule, suggests the emergence of lipid tilt texture.

## DISCUSSION

### Gb3 carbohydrate conformation

An important aspect of molecular order within GSL-containing membranes is the conformation of the carbohydrate residue. Changes to the carbohydrate orientation, which is responsible for recognition of extracellular molecules and specific ligand binding, has been shown to modulate receptor activity (29,30). Additionally, the surrounding phospholipid composition has been shown to modulate ligand binding affinity, suggesting that the membrane environment impacts carbohydrate conformation (11). Using the $\rho_{e^-}$ obtained from XR, we show that Gb3 conformation in monolayers depends on both the acyl chain structure and the local lipid environment.

**TABLE 2 Influence of Gb3 species on lipid APM[a]**

| | Gb3 species | | | | |
|---|---|---|---|---|---|
| 4:1 mixed monolayers | Mix | 22:0 | 22:1 | 14:0 | lyso |
| DSPC 30mN/m | 45.1 | 45.4 | – | 46.8 | 47.8 |
| Deviation[b] | −2.8% | −2.1% | – | +0.9% | +3.0% |
| DPPE 20mN/m | 42.6 | 42.4 | 42.6 | 42.1 | 43.1 |
| Deviation[b] | 0.0% | −0.5% | 0.0% | −1.2% | +1.2% |
| DPPE 40mN/m | 40.1 | 40.2 | 40.5 | 39.7 | 40.7 |
| Deviation[b] | −0.7% | −0.5% | +0.2% | −1.7% | +0.7% |

[a]Units of lipid APM values are Å$^2$ with uncertainty ±0.1 Å$^2$.
[b]Deviation is the percent difference between the mixed monolayer APM and the ideal mixing APM.

The Gb3 carbohydrate moiety was roughly estimated to have an extended length of 15 Å using a Universal Force Field and an energy minimization routine (31). For the pRBC Gb3 monolayer, a 17 Å thick carbohydrate region, close to the estimate for full carbohydrate extension, was modeled. The slight increase suggests that heterogeneous acyl chains result in a staggered configuration of molecules. For Gb3 analogs, the carbohydrate region thickness, a spatial and temporal averaging of carbohydrate conformations, falls in the range of 11–14 Å suggesting partial sampling of bent conformations. The carbohydrate conformation in mixed monolayers was qualitatively similar to pure Gb3 monolayers. To estimate the solvent accessible carbohydrate volume, the average volume, $V$, containing a single Gb3 carbohydrate is defined as

$$V = T_{Carb} \times 5 \text{ APM} = xV_{H_2O} + yV_{Gal},$$

where APM was obtained from GIXD and the thickness of the carbohydrate layer, $T_{Carb}$, was obtained from XR. Using known values for the volume of a water molecule, $V_{H_2O} = 30$ Å$^3$, and a galactose molecule, $V_{Gal} = 183$ Å$^3$, a relationship between the number of water molecules, $x$, and the number of sugars, $y$, in the volume was obtained (32). The measured $\rho_{e^-}$ of the carbohydrate region is defined as

$$\rho_{e^-} = \frac{xn_{H_2O} + yn_{Gal}}{V},$$

where $n_{Gal}$ is the number of electrons in a galactose molecule and $n_{H_2O}$ is the number of electrons in a water molecule. Using these equations, $y$, the average number of Gb3's sugars, which extend past the lipid headgroups, can be calculated.

For mixed monolayers of DPPE and pRBC Gb3, 3.0 sugar molecules contributed to the $\rho_{e^-}$ of the carbohydrate region indicating that the entire carbohydrate moiety is solvent accessible. On the other hand, an average of 2.3 sugars contributed to the $\rho_{e^-}$ in DSPC/Gb3 mixtures indicating that a portion of the carbohydrate is buried within the larger PC headgroup region and may not be solvent accessible. The observation of carbohydrate shielding in gel phase PC membranes is consistent with Shiga toxin binding assay results, which demonstrate that the inclusion of cholesterol in PC membranes masks the Gb3 receptor and impacts macromolecule recognition (33). In both this study and the Shiga toxin binding assays, more ordered membranes are shown to have reduced Gb3 carbohydrate accessibility. Although it is not possible to distinguish the relative role of headgroup or acyl chain length, these results suggest a mechanism for local lipid environment to influence solvent accessibility

of Gb3's carbohydrate. In a cellular context, compositional heterogeneity within the plane of the membrane, such as lipid rafts, may be capable of modulating the structure and function of Gb3. Interestingly, the outer leaflet of animal cell membranes, where Gb3 is predominantly localized, contains a high fraction of lipids with phosphocholine headgroups. Because the carbohydrates are partially shielded in this environment, recruitment of Gb3 to specific regions on the cell surface may provide a mechanism to expose and activate the Gb3 binding site.

The acyl chain structure of the Gb3 analogs also impacted carbohydrate conformation in the mixed monolayers. In the case of DPPE/Gb3 monolayers, the carbohydrate extension beyond the headgroups was significantly reduced for all the Gb3 analogs. The greatest exposure, with an average of 1.9 solvent accessible sugar groups, occurred for the 22:0 Gb3 monolayer, whereas fewer than 1.3 sugar groups were exposed for the remaining Gb3 analogs. Considering that the naturally extracted Gb3 predominantly contains species with long acyl chains (91% equal to or >C22), these findings show a correlation between acyl chain length and exposure of the GSL carbohydrate (Fig. 5 *A*). Such a correlation may also be expected to occur in bilayer membranes where interactions between long Gb3 acyl chains and the opposing lipid leaflet would serve to further extend the carbohydrate residues.

Similar trends were observed for carbohydrate conformation in mixtures composed of DSPC and Gb3 analogs. Compared to 2.3 sugar residues for the natural Gb3 extract, calculations yielded 1.6 solvent accessible sugars in monolayers containing 22:0 Gb3. Less carbohydrate was exposed in DSPC monolayers containing the shorter chain 14:0 Gb3 (1.4 residues) or the lyso Gb3 analog (1.0 residues). The largest volume of carbohydrate, 2.5 residues, was exposed in DSPC monolayers containing the 22:1 Gb3 analog (calculated using APM of the DSPC/porcine Gb3 monolayer due to lack of GIXD for this composition). Although the 22:1 Gb3 mixture was measured at 40 mN/m, the increased carbohydrate exposure in the 22:0 Gb3 mixture is significantly greater than changes resulting from the increased surface pressure (see the Supporting Material). In this case, unsaturation in the acyl chain favored carbohydrate exposure, an effect not observed in the DPPE mixtures (Fig. 5 *B*).

These results show that Gb3 acyl chain structure impacts carbohydrate conformation with the predominant trend being greater carbohydrate exposure with longer acyl chains. Such a correlation is consistent with the enhancement of Shiga toxin binding to longer acyl chain Gb3 species (34). In cellular membranes, GSLs typically have longer hydrocarbon chains than the surrounding phospholipid species and this may serve to optimize the accessibility of the carbohydrate residues. Concerning acyl chain unsaturation, the impact on carbohydrate conformation varied between the two matrix lipid environments: in DSPC monolayers the carbohydrate was highly exposed and in DPPE monolayers it was shielded. Although it is not possible to rule out contributions due to the headgroup moiety, one explanation involves the position of the unsaturation relative to the plane of the phospholipid tail methyl groups. In the 22:1 Gb3 molecule, there are 11 methylene units between the carbonyl and the unsaturation. In comparison, the hydrocarbon tails of DPPE have 14 and DSPC tails have 16 methylene units. A vertical displacement of the 22:1 Gb3 molecule by three methylene units would be sufficient to locate the unsaturation above the plane of the DPPE tail methyl groups. Such a shift would avoid the energetic penalty associated with disrupted chain packing at the cost of burying a significant portion of the carbohydrate moiety in the headgroups. For DSPC, a five methylene shift would be required to translate the unsaturation above the phospholipid tails. If the energetic penalties associated with the larger shift outweigh the penalties associated with disrupted chain packing, such a displacement would not be favorable and the carbohydrate would be more exposed. This interpretation is consistent with GIXD measurements from mixtures containing 22:1 Gb3. Although diffraction was observed for the DPPE mixture, consistent with unperturbed chain packing, the unsaturation disrupted chain packing in the DSPC mixture to such an extent that diffraction was not observed. This interpretation suggests a possible mechanism for the lipid environment to modulate Gb3 and enable transitions between a highly extended carbohydrate conformation that promotes ligand binding and, extrapolating to physiological

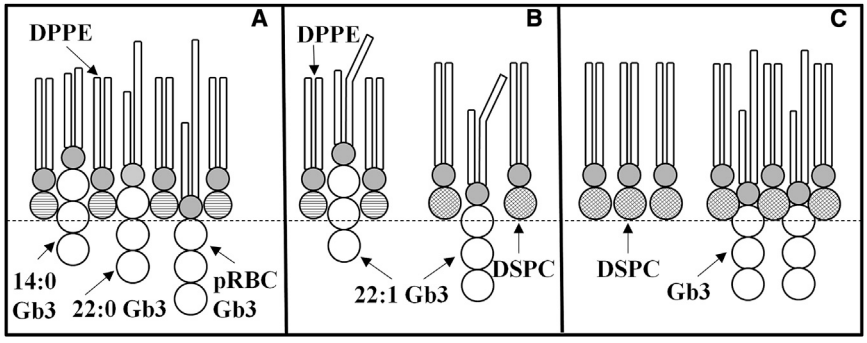


FIGURE 5 Schematic representations of the main findings concerning carbohydrate conformation and lipid condensation in monolayers containing Gb3. (*A*) Solvent accessibility and extension of the sugar groups beyond the lipid headgroups is enhanced by longer Gb3 tails. (*B*) Unsaturated Gb3 molecules impact lipid packing and carbohydrate conformation differently depending on the phospholipid environment. (*C*) In general, Gb3 condenses the packing within lipid monolayers resulting in smaller APM.

bilayers, a conformation that promotes interdigitation of the acyl chain with the opposing lipid leaflet.

### Gb3-induced lipid APM condensation

In DSPC monolayers containing pRBC Gb3, the lipid APM was more condensed than predicted for ideal mixing of the pure components with stronger condensation observed at higher $\pi$ (Fig. 5 *C*). This is consistent with the condensing effect observed in similar mixed monolayers of DPPC and GM1 (18). Despite DPPE monolayers being untilted and with small APM, condensation of the APM was also observed in higher $\pi$ DPPE/Gb3 mixtures. At reduced $\pi$, where DPPE exhibits appreciable molecular tilt, the inclusion of pRBC Gb3 did not result in a condensation of the APM. Instead, lipid packing was slightly perturbed consistent with the onset of lipid tilt texture. The emergence of tilt texture was also evident in mixtures containing 22:1 Gb3. Previously, lipid tilt texture has been observed in DPPE and GM1 monolayers when GM1 clustering was induced by cholera toxin binding (27). Although the tilt texture induced by clustering was far more dramatic than the changes observed here, these results suggest that GSLs with unsaturated chains may serve to promote tilt texture. In this case, we hypothesize that texture originates from the self-organization of nanoscale Gb3 clusters in the monolayer. The priming of tilt texture in monolayers containing unsaturated Gb3 correlates with the enhanced tubular invagination formation observed for Shiga toxin binding to this Gb3 species (12).

Substitution of the Gb3 acyl chains provided further insight into the condensation mechanism. For monolayers composed of DSPC and saturated chain Gb3 analogs, a correlation between carbohydrate extension and APM condensation was observed. In the mixture containing 22:0 Gb3, an extended carbohydrate conformation resulted in condensed APM. This can be attributed to the smaller Gb3 headgroup relieving steric repulsion between PC headgroups. On the other hand, in the mixture containing 14:0 Gb3 the APM expanded because the carbohydrate was buried within the lipid headgroup region and generated greater steric repulsion. Because the DSPC mixture containing the 22:1 Gb3 analog did not diffract, it is unclear if this correlation between APM condensation and carbohydrate extension holds for unsaturated Gb3 acyl chains. However, the lack of diffraction suggests disrupted chain packing and APM expansion which, combined with an extended carbohydrate conformation, would indicate different behavior than in the case of the saturated Gb3 analogs. Expansion of the average APM was also observed in DSPC and lyso Gb3 mixtures. In this case, the expansion is likely due to a mismatch between headgroup and tail areas promoting tilt and a concomitant APM increase.

As in the case of DSPC, unsaturated and lyso Gb3 analogs did not lead to an APM condensation in DPPE monolayers. Although DPPE/Gb3 mixtures containing saturated chain Gb3 analogs were condensed more than predicted based on ideal mixing, there was no correlation between carbohydrate conformation and APM change. This may be due to the smaller PE headgroup and the enhanced relative contribution of chain packing to APM. In the case of 22:0 Gb3, an extended carbohydrate conformation and a condensed APM were observed, which was consistent with DSPC mixtures. However, the monolayer containing 14:0 Gb3 exhibited a buried carbohydrate conformation as well as the strongest APM condensation. These results suggest that in this case close matching between the Gb3 and DPPE acyl chain structures provide the optimum conditions for APM condensation.

## CONCLUSION

Mixed monolayers of the GSL Gb3 and phospholipids were investigated at the air-water interface using XR and GIXD and compared to pure component monolayers. Both the phospholipid environment as well as Gb3 acyl chain structure effected the conformation and exposure of the carbohydrate residues. Longer acyl chains exposed more carbohydrate volume to the solvent, consistent with observations of enhanced ligand binding, suggesting that in cellular membrane the long length of GSL acyl chains relative to other membrane constituents serves to optimize receptor activity. Monolayers containing Gb3 with an unsaturated acyl chain exhibited distinctly different carbohydrate conformations depending on the phospholipid environment suggesting that in physiological membranes specific local interactions between the GSL and neighboring molecules can serve to switch between shielded and exposed carbohydrate conformations or acyl chain interdigitation states.

For many of the mixtures studied, Gb3 condensed the packing resulting in APM smaller than predicted based on ideal mixing. The condensation magnitude depended on both the phospholipid packing properties and the Gb3 acyl chain structure. In the case of DSPC mixtures, the condensation mechanism exhibited a dependence on carbohydrate conformation and headgroup interactions, whereas chain packing considerations played a more dominant role in the condensation of DPPE mixtures. These findings illuminate the complex interactions, depending on acyl chain structure and the local membrane environment, that may impact GSL partitioning within lipid rafts as well as carbohydrate conformation and receptor activity.

## SUPPORTING MATERIAL

Three figures, one scheme, supporting text, data, and references are available at http://www.biophysj.org/biophysj/supplemental/S0006-3495(14)00741-3.

We thank HASYLAB for access to the BW-1 beamline and Diamond Light Source for access to beamline I-07 (SI8072) that contributed to the results presented here. We also thank the Partnership for Soft Condensed Matter (PSCM) laboratory where Langmuir isotherm and Brewster angle microscopy measurements were performed.

This work was supported by grants from the Agence Nationale pour la Recherche (ANR-09-BLAN-283 and ANR-11 BSV2 014 03), Marie Curie Actions—Networks for Initial Training (FP7-PEOPLE-2010-ITN), and European Research Council advanced grant (project 340485). A.J.C.D. was funded by the Swedish Research Council (VR).

## REFERENCES

1. Maggio, B., M. L. Fanani, …, N. Wilke. 2006. Biophysics of sphingolipids II. Glycosphingolipids: an assortment of multiple structural information transducers at the membrane surface. *Biochim. Biophys. Acta.* 1758:1922–1944.
2. Maggio, B., F. A. Cumar, and R. Caputto. 1978. Interactions of gangliosides with phospholipids and glycosphingolipids in mixed monolayers. *Biochem. J.* 175:1113–1118.
3. Lingwood, C. A. 1996. Aglycone modulation of glycolipid receptor function. *Glycoconj. J.* 13:495–503.
4. Nyholm, P. G., and I. Pascher. 1993. Orientation of the saccharide chains of glycolipids at the membrane surface: conformational analysis of the glucose-ceramide and the glucose-glyceride linkages using molecular mechanics (MM3). *Biochemistry.* 32:1225–1234.
5. Mehlhorn, I. E., E. Florio, …, C. W. M. Grant. 1988. Evidence that trans-bilayer interdigitation of glycosphingolipid long chain fatty acids may be a general phenomenon. *Biochim. Biophys. Acta.* 939:151–159.
6. Boggs, J. M., and K. M. Koshy. 1994. Do the long fatty acid chains of sphingolipids interdigitate across the center of a bilayer of shorter chain symmetric phospholipids? *Biochim. Biophys. Acta.* 1189:233–241.
7. Lingwood, D., and K. Simons. 2010. Lipid rafts as a membrane-organizing principle. *Science.* 327:46–50.
8. Simons, K., and E. Ikonen. 1997. Functional rafts in cell membranes. *Nature.* 387:569–572.
9. Lingwood, C. A., B. Binnington, …, D. R. Branch. 2010. Globotriaosyl ceramide receptor function - where membrane structure and pathology intersect. *FEBS Lett.* 584:1879–1886.
10. Simons, K., and M. J. Gerl. 2010. Revitalizing membrane rafts: new tools and insights. *Nat. Rev. Mol. Cell Biol.* 11:688–699.
11. Arab, S., and C. A. Lingwood. 1996. Influence of phospholipid chain length on verotoxin/globotriaosyl ceramide binding in model membranes: comparison of a supported bilayer film and liposomes. *Glycoconj. J.* 13:159–166.
12. Römer, W., L. Berland, …, L. Johannes. 2007. Shiga toxin induces tubular membrane invaginations for its uptake into cells. *Nature.* 450:670–675.
13. Chinnapen, D. J. F., W. T. Hsieh, …, W. I. Lencer. 2012. Lipid sorting by ceramide structure from plasma membrane to ER for the cholera toxin receptor ganglioside GM1. *Dev. Cell.* 23:573–586.
14. Arnold, T., C. Nicklin, …, M. Burt. 2012. Implementation of a beam deflection system for studies of liquid interfaces on beamline I07 at Diamond. *J. Synchrotron Radiat.* 19:408–416.
15. Parratt, L. G. 1954. Solid surface studies by total reflection of x-rays. *Phys. Rev.* 95: 617–617.
16. Alsnielsen, J., D. Jacquemain, …, L. Leiserowitz. 1994. Principles and applications of grazing-incidence x-ray and neutron-scattering from ordered molecular monolayers at the air-water-interface. *Phys. Rep.* 246:252–313.
17. Kjaer, K. 1994. Some simple ideas on x-ray reflection and grazing-incidence diffraction from thin surfactant films. *Physica B.* 198:100–109.
18. Frey, S. L., E. Y. Chi, …, K. Y. C. Lee. 2008. Condensing and fluidizing effects of ganglioside GM1 on phospholipid films. *Biophys. J.* 94:3047–3064.
19. Majewski, J., T. L. Kuhl, …, G. S. Smith. 2001. Packing of ganglioside-phospholipid monolayers: an x-ray diffraction and reflectivity study. *Biophys. J.* 81:2707–2715.
20. Miller, C. E., D. D. Busath, …, J. Majewski. 2008. Integration of ganglioside GT1b receptor into DPPE and DPPC phospholipid monolayers: an X-ray reflectivity and grazing-incidence diffraction study. *Biophys. J.* 95:3278–3286.
21. Maggio, B., F. A. Cumar, and R. Caputto. 1981. Molecular behavior of glycosphingolipids in interfaces - possible participation in some properties of nerve membranes. *Biochim. Biophys. Acta.* 650:69–87.
22. Bianco, I. D., G. D. Fidelio, and B. Maggio. 1988. Effect of glycerol on the molecular-properties of cerebrosides, sulfatides and gangliosides in monolayers. *Biochem. J.* 251:613–616.
23. McIntosh, T. J. 1980. Differences in hydrocarbon chain tilt between hydrated phosphatidylethanolamine and phosphatidylcholine bilayers. A molecular packing model. *Biophys. J.* 29:237–245.
24. Dörfler, H. D. 1990. Mixing behavior of binary insoluble phospholipid monolayers. Analysis of the mixing properties of binary lecithin and cephalin systems by application of several surface and spreading techniques. *Adv. Colloid Interface Sci.* 31:1–110.
25. Miller, C. E., J. Majewski, …, T. L. Kuhl. 2008. Probing the local order of single phospholipid membranes using grazing incidence x-ray diffraction. *Phys. Rev. Lett.* 100:058103.
26. Sun, W. J., S. Tristram-Nagle, …, J. F. Nagle. 1996. Structure of gel phase saturated lecithin bilayers: temperature and chain length dependence. *Biophys. J.* 71:885–891.
27. Watkins, E. B., C. E. Miller, …, T. L. Kuhl. 2011. Membrane texture induced by specific protein binding and receptor clustering: active roles for lipids in cellular function. *Proc. Natl. Acad. Sci. USA.* 108:6975–6980.
28. Watkins, E. B., C. E. Miller, …, J. Majewski. 2009. Structure and orientational texture of self-organizing lipid bilayers. *Phys. Rev. Lett.* 102:238101.
29. Lingwood, D., B. Binnington, …, K. Simons. 2011. Cholesterol modulates glycolipid conformation and receptor activity. *Nat. Chem. Biol.* 7:260–262.
30. Strömberg, N., P. G. Nyholm, …, S. Normark. 1991. Saccharide orientation at the cell surface affects glycolipid receptor function. *Proc. Natl. Acad. Sci. USA.* 88:9340–9344.
31. Hanwell, M. D., …, G. R. Hutchison. 2012. Avogadro: an advanced semantic chemical editor, visualization, and analysis platform. *J. Cheminform.* 4:17.
32. Origlia, M. L., T. G. Call, and E. M. Woolley. 2000. Apparent molar volumes and apparent molar heat capacities of aqueous D-glucose and D-galactose at temperatures from 278.15 K to 393.15 K and at the pressure 0.35 MPa. *J. Chem. Thermodyn.* 32:847–856.
33. Mahfoud, R., A. Manis, …, C. A. Lingwood. 2010. A major fraction of glycosphingolipids in model and cellular cholesterol-containing membranes is undetectable by their binding proteins. *J. Biol. Chem.* 285:36049–36059.
34. Kiarash, A., B. Boyd, and C. A. Lingwood. 1994. Glycosphingolipid receptor function is modified by fatty acid content. Verotoxin 1 and verotoxin 2c preferentially recognize different globotriaosyl ceramide fatty acid homologues. *J. Biol. Chem.* 269:11138–11146.